Effect Of Gamma Radiation On Carbon Steel Corrosion

K. Daub, J.C. Wren

Department of Chemistry, the University of Western Ontario, London, Ontario

ABSTRACT

An important factor influencing the aging of nuclear reactor coolant piping and the transport of activation products in the piping is the chemical effects of ionizing radiation on steel corrosion. In the presence of ionizing radiation (e.g., gamma radiation), water decomposes into both oxidizing and reducing species (e.g., •OH, H_2O_2, O_2^-) whose net interactions with steels are not fully understood. The effect of radiation on the corrosion kinetics of carbon steel was studied by following the corrosion potential, E_{CORR}, of a carbon steel electrode during its exposure to γ-radiation. The changes in the surface film composition and morphology due to radiation were studied using Electrochemical Impedance Spectroscopy (EIS). The gas and aqueous samples were analyzed for H_2, O_2, and H_2O_2 using a GC-MS/TCD (Gas Chromatography-Mass Spectrometer/Thermal Conductivity Detector) and UV-visible spectrophotometer, respectively. The results of the radiation study were then compared with those obtained with carbon steel exposed to H_2O_2 under non-irradiation conditions. The comparison indicates that the main influence of gamma radiation on carbon steel corrosion is via the radiolytic production of H_2O_2 in the aqueous phase.

KEYWORDS

Corrosion kinetics, carbon steel, water radiolysis, gamma radiation, corrosion potential, passive oxide films, impedance spectroscopy

1. INTRODUCTION

With the potentially dire near future due to global warming, the scientific community has spent a great deal of time and effort researching alternatives to the current reliance on fossil fuels. Nuclear power has the ability to supply the large energy demands of the world while releasing no greenhouse gases. The Canadian-designed CANDU type nuclear reactors are currently contributing approximately 16 % of electricity generation in Canada, and approximately 45 % in Ontario.

CANDU reactors use natural (un-enriched) uranium fuel that is formed into small pellets and inserted into the reactor core as fuel bundles. CANDU reactors are capable of using non-enriched uranium because they use heavy water as a moderator. The moderator slows down the neutrons and, hence, promotes the fission of uranium atoms. The heat transport system (HTS) also contains heavy water and carries the heat released from the reactor core to the steam generator along a temperature gradient of about 270°C to 310°C. The HTS includes an array of zirconium alloy tubes in the reactor core that are connected to the coolant pumps and steam generators with feeder pipes made of carbon steel [1].

Degradation of the carbon steel feeder pipes is an operational and safety concern for the nuclear power industry. While very resistant to degradation through corrosion under the CANDU coolant chemistry conditions (pH~10 controlled by LiOH addition and low corrosion potential controlled by H_2 addition), the carbon steel will inevitably be exposed to water radiolysis products within the coolant (since the coolant passes through the high radiation field in the reactor core). Water can degrade under high energy irradiation as follows [2]:

$$H_2O \quad \rightarrow \quad \bullet OH,\ e_{aq}^{-},\ H\bullet,\ HO_2\bullet,\ H_2,\ H_2O_2,\ H^{+} \tag{1}$$

It can be seen that a number of reactive oxidizing and reducing species are produced, all of which can affect the local oxidation potential of the coolant and corrosion of carbon steel [3,4]. It has been found that H_2O_2 and $\bullet OH$ are key water radiolysis products. The soluble products of carbon steel corrosion, especially Fe^{2+}, will also interact with water radiolysis products [5]

$$Fe^{2+}(aq) \underset{\bullet H,\ e_{aq}^{-},\ \text{or}\ \bullet O_2^{-}}{\overset{\bullet OH,\ H_2O_2,\ \text{or}\ O_2}{\rightleftarrows}} Fe^{3+}(aq) \tag{2}$$

The reactions of soluble iron species will have an effect on the balance of radiolytic species in solution and the composition of the corroding surface (the surface of the carbon steel is in general coated with a layer of magnetite (Fe_3O_4) that provides resistance to corrosion). The oxidation of soluble Fe^{2+} could lead to passivation of the corroding carbon steel surface since Fe^{3+} species are very insoluble, and, in general, the solubility of iron oxide/hydroxide species decreases as follows [6,7,8].

$$Fe(OH)_2 \gg FeOOH > Fe_3O_4 > Fe_2O_3 \tag{3}$$

A representation of the overall synergistic circuit is represented in Figure 1.

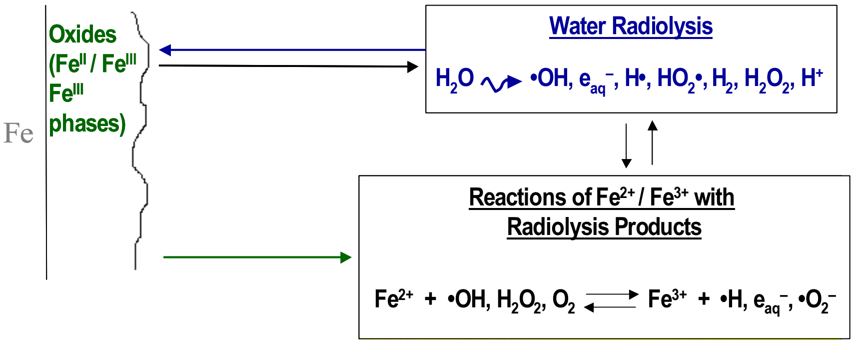

Figure 1: Synergistic Circuit of Carbon Steel, Soluble Fe^{2+}, and Water Radiolysis Products.

The parameters affecting corrosion are temperature, pressure, pH, composition of the electrolyte, radiation dose, radiolysis products concentrations, and the morphology of the oxides formed on the carbon steel. Our research is focused on the kinetics and mechanism of corrosion of various oxide films under controlled radiation doses at room temperature. Gas and aqueous samples of the system were analyzed for H_2, O_2, and H_2O_2, using a Gas Chromatography (GC) equipped with Mass Selective, Thermal Conductivity, and Electron Capture detectors (MSD/TCD/ECD) for O_2 and H_2 analysis and a UV-visible spectrophotometer for H_2O_2 analysis. Finally, electrochemical techniques were used to analyze the redox reactions involved in the formation of oxide films, and their reaction with radiolysis products.

2. EXPERIMENTAL

2.1 Electrochemical Setup and Conditions

A three-electrode system, consisting of a working electrode (WE), a reference electrode (RE), and a counter electrode (CE) was used, Figure 2. The WE was made of carbon steel with an exposed surface area of 0.785cm^2, and the CE was a platinum mesh-wire. The RE was an Hg/HgO Electrode in 1.0 M KOH solution, which has shown to be more resistant to radiation than the saturated calomel electrode (SCE) or Ag/AgCl$_2$ electrode. The potential of the RE is 0.37 V versus the Standard Hydrogen Electrode (SHE). Although data was obtained using an Hg/HgO reference electrode, all potential values are quoted against SCE to facilitate comparison to other literature values. The potential of an Hg/HgO reference electrode against SCE is 0.13 V.

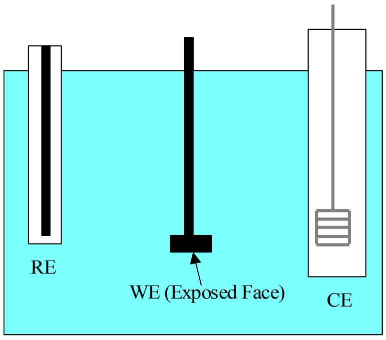

Figure 2: Schematic Layout of Three-electrode Cell, Containing a Working Electrode (WE), a Reference Electrode (RE), and a Counter Electrode (CE).

All solutions were made using ultrapure water with a conductivity of 18.2 MΩ-cm obtained from a Milli-Q Millipore system. All experiments were performed at pH 10.6 in 0.01 M borate ($Na_2B_4O_7$) solutions at room temperature. The solution is buffered to pH 10.6 since the coolant in CANDU HTS is maintained at ~10.6, where the amount of soluble iron products is minimized. A pH of 10.6 was obtained by adding an appropriate amount of 1 M NaOH solution to the borate solution. Argon gas purging for one hour was used to eliminate dissolved oxygen before beginning each experiment. Hydrogen peroxide solutions were prepared from a 3 % wt. stock solution using a micropipette (39.68 uL), yielding hydrogen peroxide concentrations of 7.0×10^{-5} M in a 500 mL solution.

The electrode system was irradiated in an MDS Nordion Gammacell 220 Excel, which has ^{60}Co pencils for the radiation source, having a half-life of 5.3 years. ^{60}Co emits γ-rays at energies of 1.17 and 1.33 MeV and emits β-particles with an energy of 318 keV (but these are blocked) [9]. The absorbed dose in water was determined by the Fricke dosimetry to be ~ 2.4 Gy/s.

All corrosion potential measurements were performed using an 8 channel Solartron 1480 potentiostat. Corrware™ and Corrview software (supplied by Scribner and Associates) was used to control experiments and analyze data. The frequency analyzer used for Electrochemical Impedance Spectroscopy (EIS) measurements and analyses was a Solartron Frequency Response Analyzer 1255B. The frequency range in all EIS measurements was 10^{-2} to 10^{4} Hz.

2.2 Experimental Procedure

The general experimental procedure is shown graphically in Figure 3.

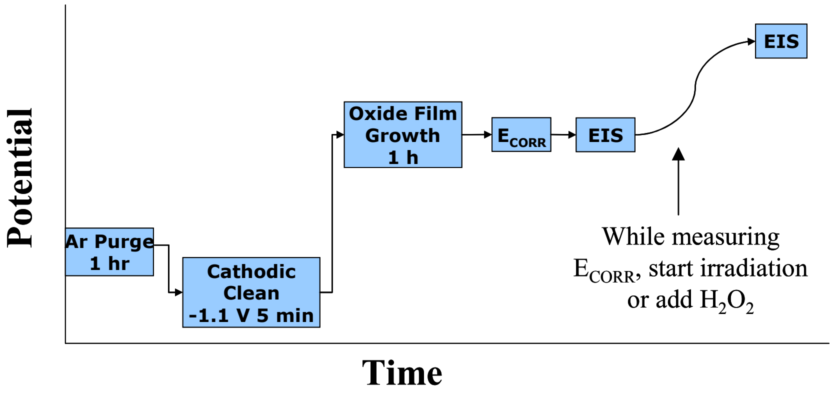

Figure 3: Experimental Procedure for Determining the Effects of Irradiation, or H_2O_2 Addition on Potentiostatically Grown Carbon Steel Oxide Films in 0.01 M Borate Solution at pH 10.6, 25°C.

All experiments began with 1 h argon purge to remove any oxygen in the solution, followed by cathodic cleaning by applying a potential of -1.1 V (vs. SCE, or -0.97 vs. Hg/HgO) for 5 minutes. This low potential removes any air-formed oxides on the working electrode, thereby creating a clean metal surface. Various potentials were then applied for one hour (-1.1, -0.58, -0.23, 0.3 V vs. SCE) to grow films with different compositions and properties. These potentials were chosen by reference to cyclic voltammetry experiments, which indicate the changes in behaviour of the steel at different potentials, see Figure 4 in Section 3. The corrosion potential was then measured for one hour while the system approached steady state, and an EIS measurement was performed at the steady-state E_{CORR}. Measuring EIS against the steady-state E_{CORR} implies the sinusoidal potential of ± 10 mV was against E_{CORR} and the current response was determined. After this first impedance measurement, the electrochemical cell and potentiostat setup were either transferred to the Gammacell for irradiation studies or remained inside the Faraday cage for H_2O_2 studies. Total irradiation times were 2 h, occurring while E_{CORR} was monitored for 3.5 h. The time delay between the EIS and the onset of the irradiation or H_2O_2 addition was approximately 15 min. Following irradiation the system achieved steady state, and another set of EIS measurements was made at steady-state E_{CORR} to compare the EIS before and after irradiation or hydrogen peroxide addition. Samples for Spectrophotometric and Gas Chromatography analysis were also taken before and after the 3.5 h E_{CORR} measurement.

3. RESULTS AND DISCUSSION

3.1 Oxidation Regions of Carbon Steel

Cyclic voltammetry was first performed on carbon steel, Figure 4, for the purpose of providing a basis for interpreting the potentiostatic film growth and EIS measurements. Cyclic voltammetry involves scanning the potential range linearly and measuring the current response to characterize oxidation ranges of carbon steel [10]. For our experiment the potential range was scanned from –1.1 V to 0.4 V for 3 full cycles. For the first cycle five distinct anodic peaks were observed on the forward scan (A1 through A5). Similar results, with slightly different behaviour have been observed over a range of pH values [11,12,13]. Upon subsequent cycles, the anodic peak, A3, became very sharp and clear, and the cathodic peaks, C1 and C2, began to increase. The assignments of the peaks to various iron oxidation and reduction processes are discussed in detail elsewhere [14]. Only a brief description is given here.

The peak A1 (a shoulder at ~ –0.9 V) was only seen for the first cycle, and attributed to the reoxidation of hydrogen absorbed in the electrode during cathodic cleaning [13]. The broad peak (A2) observed in the potential region of –0.9 V to –0.6 V encompasses the formation of $Fe(OH)_2$ and Fe_3O_4 (magnetite) and the conversion of $Fe(OH)_2$ to α-FeOOH. Peak A3 is very sharp and occurs over a narrow range, which suggests a rapid reaction to produce an insulating layer on the steel surface. Based on the equilibrium potentials of iron and its oxides, and the stability of hematite (Fe_2O_3), the reaction is attributed to the conversion of $Fe_3O_4 \rightarrow \gamma\text{-}Fe_2O_3$. Upon subsequent cycles the anodic peak A3 increased in size, which is consistent with the accumulation of Fe_3O_4 and its oxidation (at least partially) to γ-Fe_2O_3. The peak A3 also involved the formation of another γ-Fe^{III} species, γ-FeOOH, due to the conversion of $Fe(OH)_2$. Peak A4 could be attributed to the oxidation of Fe^{II} species ($Fe^{2+}$and $Fe(OH)_2$) to α-FeOOH. Peak A4 lied at a potential (~ –0.2 V) much higher than the equilibrium potential for the conversion of $Fe(OH)_2$ to α-FeOOH, which would result from a kinetically slow anodic process [15,16]. The very shallow anodic peak, A5, over the potential range 0 to 0.4 V is attributed to the further production of γ-FeOOH due to the conversion from Fe_3O_4. Upon reversal of the scan two cathodic peaks were observed (C1 and C2), which are attributed to the reduction of γ-FeOOH (C1) and γ-Fe_2O_3 (C2).

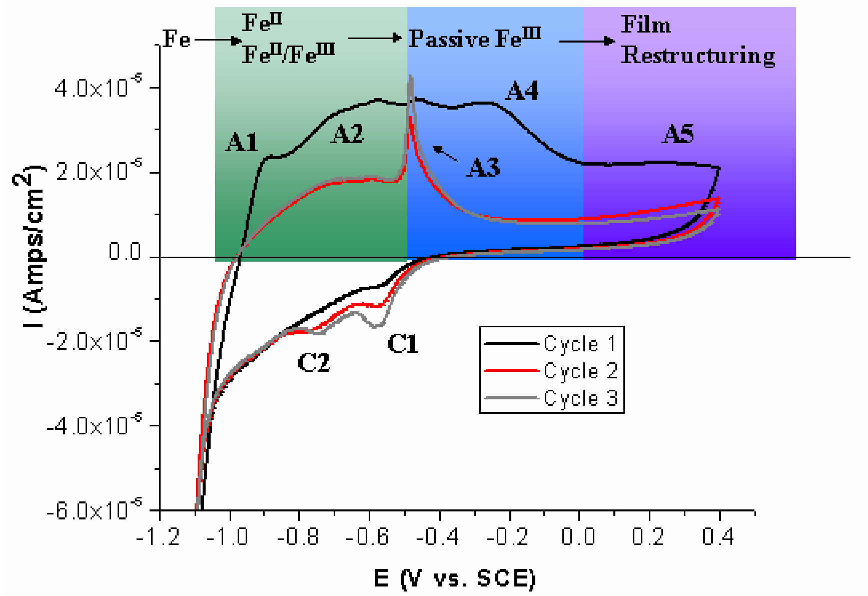

Figure 4: Cyclic Voltammograms Recorded on Carbon Steel in Ar-Purged 0.01 M Borate Solution at pH 10.6, 25°C and at a Scan Rate of 5mV/s.

In general, the oxidation behaviour of carbon steel in borate solutions at pH = 10.6 can be divided into three distinct regions. Region I occurs at potentials less than –0.5 V, where the surface of iron is active and only partially covered by $Fe(OH)_2$ and/or Fe_3O_4. Region II is in the potential range from –0.5 V to 0 V, and in this region iron is passivated with two oxide layers. The outer layer is composed of γ-Fe_2O_3 and γ-FeOOH and the inner layer of a Fe^{II}/Fe^{III} oxide/hydroxide. Finally, Region III is at potentials greater than 0 V when further conversion of Fe_3O_4 to γ-FeOOH can cause some oxide film restructuring and slight film breakdown.

In other studies conducted in our laboratory, it has been found that the E_{CORR} of anodically formed films relaxes to one of the three pseudo steady-state values occurring in regions I and II. The three pseudo steady-state values occur roughly at –0.8 V, -0.6 V, and –0.5 V. For a clean CS surface, the steady-state E_{CORR}, in general, reaches ~ -0.8 V, which is established from the oxidation of Fe to Fe^{II} or $Fe^{II/III}$ species coupled with the reduction of H_2O to H_2. For the films grown at potentials in Region II, the E_{CORR} of the system, in general, first reached ~ -0.6 V, close to an equilibrium potential for the Fe_3O_4 and Fe_2O_3, and upon further relaxation, reached ~ -0.8 V:

$$2Fe_3O_4 + H_2O \rightarrow 3Fe_2O_3 + 2H^+ + 2e \qquad E_{eq} = -0.648\ \text{V (at pH=10.6)} \qquad (4)$$

The steady-state E_{CORR} for the films grown in Region III initially reached -0.5 V, where the galvanic coupling between the reduction of FeOOH to Fe_3O_4 and the oxidation of Fe_3O_4 to Fe_2O_3 was possible. At longer times, the E_{CORR} then further relaxes to -0.6 and to -0.8 V. This shows that prior to irradiation all systems, except for the films grown at –1.1 V, reached an initial pseudo steady-state E_{CORR} value in the ~ -0.6 V and -0.5 V range, with the actual value somewhat depending on the initial film growth potential. Although all systems relaxed to a pseudo steady-state E_{CORR} soon after potentiostatic film growth, a longer open circuit time could lead to further relaxation to a lower real steady-state value.

3.2 Effect of Irradiation on E_{CORR} and Solution Redox Conditions

The corrosion of metal can be considered of consisting of two half reactions, oxidation of metal species coupled with the reduction of aqueous species. The system consisting of the two half reactions soon achieves a steady-state potential. This potential defined as the corrosion potential (E_{CORR}), sometimes referred to as the open circuit potential, or electrochemical corrosion potential (ECP), is the potential at which the system achieves charge balance. Due to the charge balance, the currents of the net anodic and net cathodic reactions at E_{CORR} must be opposite in sign but equal in magnitude. These currents at E_{CORR} are referred to as the corrosion current, i_{CORR} (i.e., $|\Sigma i_a| = |\Sigma i_c| = i_{CORR}$). Since this current is a measure of the rate of a reaction, the carbon steel degradation can be determined if i_{CORR} can be measured. However, due to mass and charge balance, electrons are contained within a short circuit, resulting in zero net current, and the corrosion current cannot be measured directly. Nevertheless, the corrosion current as a function of E_{CORR} can be independently established using electrochemical analysis techniques. If this current-potential relationship is established and the E_{CORR} values achieved can be estimated, the corrosion rate of a given system can be determined.

Table 1 summarizes the changes in E_{CORR} for various oxide films and the concentrations of redox species, after a 2 h irradiation period.

Table 1: Change in E_{CORR} and Concentrations of Radiolysis Products Produced*

E_{APP} Vs. SCE (V)	E_{CORR} Pre Irradiation	E_{CORR} Post Irradiation	$[H_2O_2]$ x10^{-5} (M)	O_2 %	H_2 %
-1.1	-0.63	-0.37	6.98	2.19	1.08
-1.1	-0.71	-0.43	6.1	2.88	1.41
-1.1	-0.82	-0.44	5.76	3.19	1.44
-0.58	-0.56	-0.34	6.43	2.40	1.12
-0.58	-0.57	-0.41	6.47	3.73	1.28
-0.23	-0.56	-0.38	5.65	3.13	1.37
-0.23	-0.57	-0.34	5.76	3.17	1.22
-0.23	-0.54	-0.36	6.8	6.38	1.16
0.3	-0.63	-0.35	5.37	0.95	1.52
0.3	-0.51	-0.35	8.78	16.69	0.44
0.3	-0.52	-0.39	7.25	4.48	1.07

* Carbon Steel Sample in 0.01 M Borate Solution at pH 10.6, 25°C Following an Irradiation Period of 2h.

Prior to irradiation, all E_{CORR} values fell close to one of the three E_{CORR} values expected (-0.8, -0.6, and -0.5 V). Electrodes cathodically cleaned at –1.1 V, and hence free of an oxide film, exhibited the lowest E_{CORR} value around –0.8 V, while oxide films grown at various other applied potentials fell within the pseudo steady-state regions of –0.6 and –0.5 V. Due to shorter relaxation times on measuring E_{CORR} the oxide films grown at various applied potentials fell to the pseudo steady-state E_{CORR} values, and not the eventual relaxation value of –0.8 V. The similarities in films grown at different potentials can be seen from the similar steady-state E_{CORR} values ~ –0.35 V achieved after irradiation. Although the films grown at different potentials had different properties and each film relaxed on open circuit via a different pathway, they all reached a similar final steady-state E_{CORR}. The cathodically cleaned, oxide-free carbon steel samples were slightly different, and relaxed to a slightly lower potential around –0.45 V. Examples of the changes in E_{CORR} as a function of irradiation time for different oxide-covered films are shown in Figure 5.

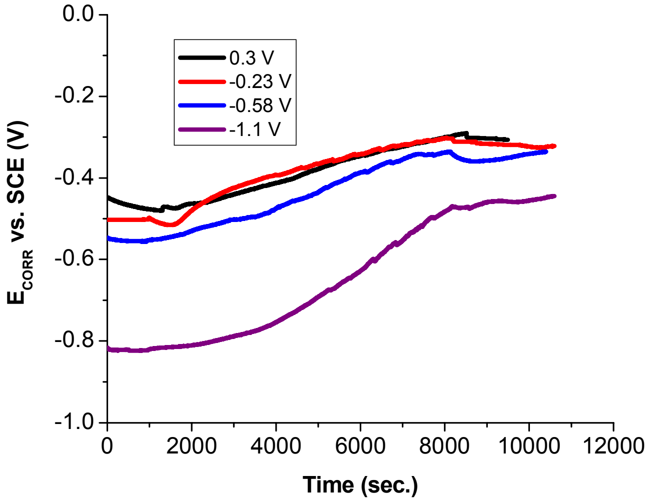

Figure 5: Time Dependent Behaviour of E_{CORR} on Oxide-Covered Carbon Steel Observed During 2 h Irradiation in the Gamma Cell: Films grown for 1 h at -1.1 V, -0.23 V, -0.58 V, and -1.1 V (vs. SCE). Irradiation started at ~ 1000 seconds, and ended at 8200 seconds.

3.3 Production of Water Radiolysis Species

Using the water radiolysis model developed by Wren et. al [5], the production of H_2O_2 by γ-radiation at the absorbed dose rate of 2.4 Gy/s was calculated as a function of irradiation time. Blank cells (a cell containing all components, except a carbon steel working electrode) were irradiated for different times and the analyzed H_2O_2 concentrations were found to match the calculated results closely, justifying the model, Figure 6.

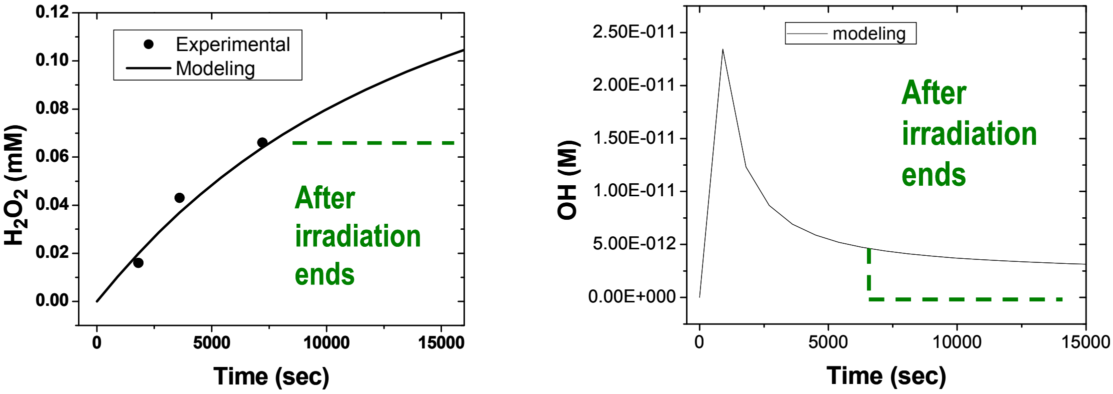

Figure 6: (a): H_2O_2 Production with Irradiation Time: The model calculation results (solid line) are compared with the experimental data obtained in a blank cell. (b): Calculated •OH Production with Irradiation Time. The calculated •OH concentration following the completion of 2 h irradiation is also shown.

Also of note is that the change in E_{CORR} with irradiation time exhibited the same gradual change with time obtained for the production of H_2O_2 with irradiation time. This demonstrates the overriding importance of H_2O_2 as a water radiation-induced redox species. Once irradiation ended [H_2O_2] can decrease via thermal decomposition over time, but this rate is very slow at room temperature. It is possible that •OH contributed to E_{CORR}, but its overall effects appeared to be much smaller than that of H_2O_2. Modeling of •OH production showed a large drop in concentration over time, and a decay to zero once irradiation stops, Figure 6. This loss of •OH once irradiation stopped may have given rise to the slight dip of E_{CORR} to lower potentials immediately following termination of irradiation which was seen for many E_{CORR} measurements before steady-state was achieved (Figure 5).

Analyses of the redox species produced after irradiation was complete showed that all concentrations are similar, irrespective of film growth potential. Most importantly, for almost all 2 h irradiation experiments the concentration of H_2O_2 was very close to 7.0×10^{-5} M. Also, gas phase analyses yielded $O_{2(g)}$ concentrations from 2 to 3 %, and $H_{2(g)}$ concentrations from 1 to 1.5 %. An exception to this occurred for oxide films grown at 0.3 V, where concentrations varied to a greater degree. One potential explanation for this observation is that the reduction of γ-FeOOH to Fe_3O_4 is coupled with the oxidation of H_2O_2 to O_2, thus explaining the higher concentrations of O_2 for films grown at 0.3 V.

3.4 Comparison of Irradiated and Non-irradiated Systems

Studies on the effects of H_2O_2 addition to the system were done in two ways. First, H_2O_2 was added in various concentrations ranging from 1×10^{-5} M to 1×10^{-2} M, to determine the influence of concentration on E_{CORR} (for films grown at –0.25 V vs. SCE), and secondly, H_2O_2 concentrations closely matching those produced by irradiation were added to the system to compare E_{CORR} changes for irradiated and non-irradiated systems.

Upon addition of H_2O_2, E_{CORR} increased sharply and then changed more slowly to reach a steady-state value in all cases. This was due to hydrogen peroxide reduction shifting to a higher potential, and therefore E_{CORR} follows with a shift to balance currents. Generally, for higher concentrations of H_2O_2, the steady-state E_{CORR} was achieved almost immediately with little to no change during the experiment. However, with the addition of lower concentrations of H_2O_2, E_{CORR} showed a more gradual change over the course of the experiment, Figure 7. Previous studies have shown that the time-dependent behaviour of E_{CORR} is a function of the film growth potential as well as the H_2O_2 concentration [14].

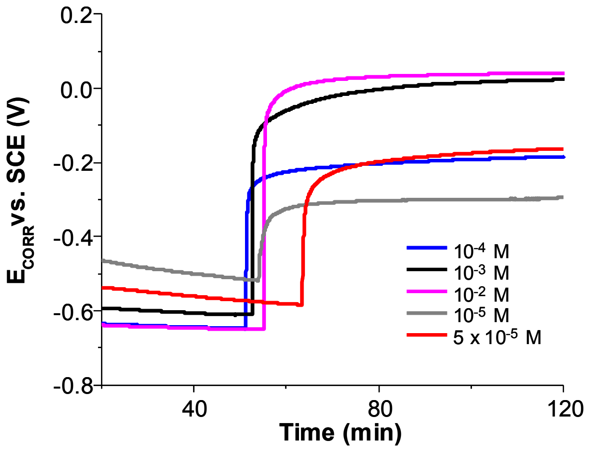

Figure 7: A Measure of the Change in E_{CORR} for Films Grown at –0.25 V vs. SCE for the First Hour Following the Addition of Varying H_2O_2 Concentrations.

After the first two hours of the measurement, E_{CORR} values varied gradually to reach their steady-state values once the experiments were stopped after a total E_{CORR} measurement of 14 hours. The final steady-state value was seen to be a function of H_2O_2 concentration for concentrations less than 1 x 10^{-3} M, but independent of the initial film growth potential, Figure 8. A likely reason why the final steady-state value was independent of H_2O_2 concentrations at high concentrations is that the hydrogen peroxide ability to act as an either an oxidant or a reductant. Due to the unknown dissolved O_2 concentration, the equilibrium potential for the half reaction (6) is difficult to determine precisely. However, it is feasible that the E_{CORR} value observed at $[H_2O_2] > 10^{-3}$ M is more oxidizing than the E_{eq} of (6) [17].

$$2\,H_2O_2 + 2\,e^- \rightarrow 2\,OH^- \qquad E^o = 2.02\text{ V(vs. SCE)} \tag{5}$$
$$H_2O_2 \rightarrow O_{2(g)} + 2\,H^+ + 2\,e^- \qquad E^o = -0.44\text{ V (vs. SCE)} \tag{6}$$

This results in the reduction reaction, and in turn limits the corrosion potential at a hydrogen peroxide concentration above 1 x 10^{-3} M.

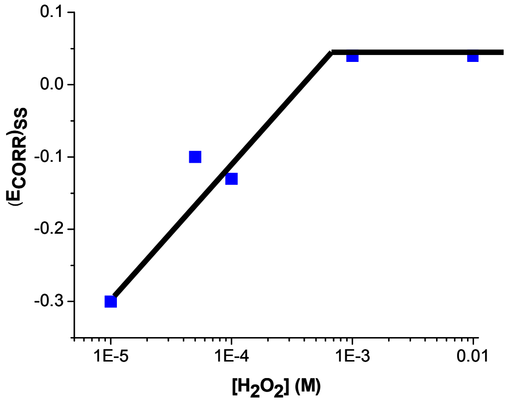

Figure 8: Final E_{CORR} Steady-state Values for Films Grown at –0.25 V vs. SCE as a Function of $[H_2O_2]$.

To match concentrations of H_2O_2 produced by irradiation, H_2O_2 was added at an initial concentration of 7 x 10^{-5} M. Although E_{CORR} showed a much steeper climb for the non-irradiated exposure, both non-irradiated and irradiated E_{CORR} values reached similar steady-state values, irrespective of initial film growth. Also, comparison of a single H_2O_2 addition to one involving multiple steps to achieve the same overall concentration showed the steady-state E_{CORR} values are identical, Figure 9. The stepwise addition of H_2O_2 more closely approached the behaviour observed for an irradiated sample since H_2O_2 was continually and gradually being produced under irradiation. Although addition in multiple steps followed the irradiated E_{CORR} change closer, the initial and final states for irradiated, single step H_2O_2 addition, or multi step H_2O_2 addition were all the same.

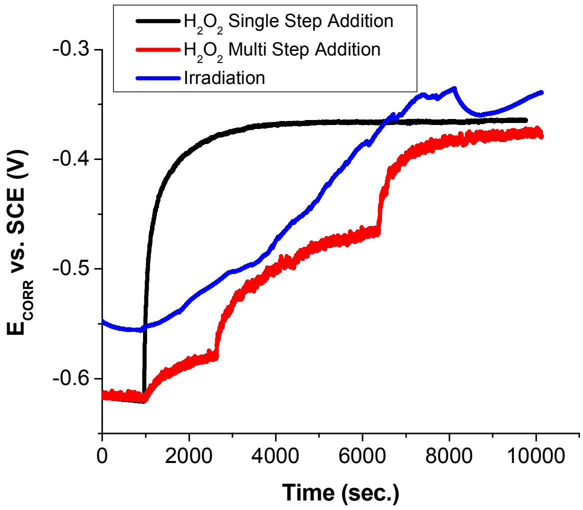

Figure 9: Comparison of the Effects of Radiation and H_2O_2 on the Time-Dependent E_{CORR} Behaviour Observed with the Oxide Film Grown at -0.58 V for 1 h. H_2O_2 was added in single or multiple steps to a final concentration of 7.0×10^{-5} M.

3.5 Electrochemical Impedance Spectroscopy Summary

The electrochemical system of oxide-covered carbon steel and solution can be represented by a series of impedance values (i.e., a combination of resistance and capacitance). An electrode interface system is rarely purely resistive or capacitive, but instead is a mixture of the two. In general, resistance results from a surface film (in this case iron oxides) and solution resisting the flow of charged species (electrons, ions, and ion vacancies), and capacitance from the build up of charges at the metal/metal oxide, and/or oxide/solution interfaces. The resistance and capacitance of a surface film will depend on the composition and morphology of the film, and measurements of the capacitance and resistance provide valuable insight into the film formation kinetics. Electrochemical Impedance Spectroscopy (EIS) was used to determine the film resistance and capacitance. EIS involves applying a small sinusoidal voltage (± 10 mV) to the working electrode and measuring the resulting sinusoidal current response [10,18]. The amplitude and the phase angle shift of the resulting current provide the resistive and capacitive component of an electrochemical system.

When there is more than one RC component in the circuit, the resistance and capacitance of individual components can be extracted from the impedance measurements as a function of the frequency of the sinusoidal potential input. Qualitatively, the impedance as a function of the frequency can be used to give an idea of how the system is behaving. For example, at very high frequencies there is no time for the charge to build up a capacitance, so the impedance is purely resistive, and specifically, the solution resistance can be determined. At very low frequencies the capacitance has time to build up and dissipate, and the resulting impedance measurement is due to the total resistance of the system. In between the low and high frequencies, both resistance and capacitance will contribute to the impedance. Quantitatively, the data can be fit by an equivalent circuit model, which consists of a series of RC components, representing the electrochemical system. Once an appropriate, and generally the simplest possible, model is found, the individual elements of the circuit can be determined. The circuit elements are then used to determine the specific surface resistance and capacitance and the solution resistance.

An example of the EIS recorded on an irradiated carbon steel electrode is shown in Figure 10.

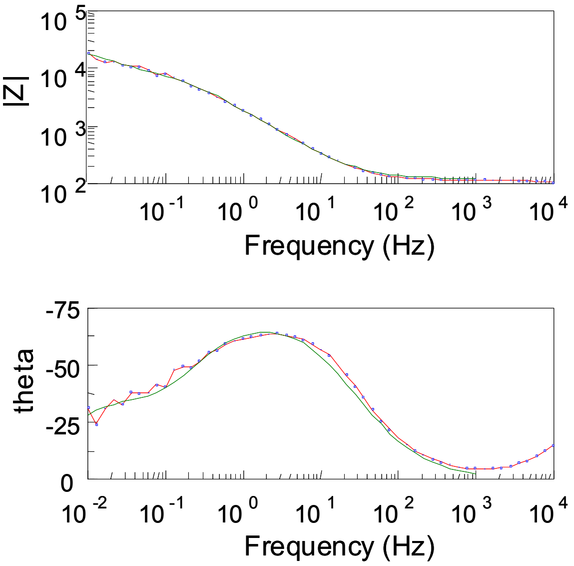

Figure 10: Bode Plot of the EIS Recorded on the Irradiated Carbon Steel Specimen. The green line is the fit from the circuit, and the red line is experimental data for a film grown at –0.23V vs. SCE after 2 h irradiation.

Previous studies in our laboratory have found a dual-layer (or two RC components) equivalent circuit, Figure 11, best represents oxide-covered carbon steel systems [14]. This circuit represents a carbon steel surface with two oxide layers, outer Fe^{III} oxide layer and inner Fe^{II}/Fe^{III} oxide layer, each composed of a resistance and a capacitance.

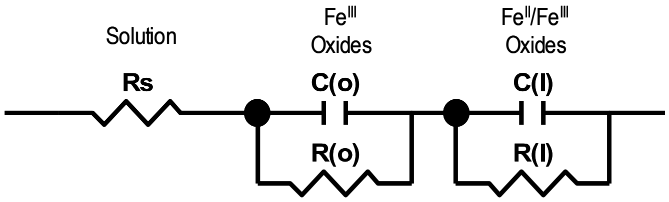

Figure 11: Equivalent Circuit Representation for the Dual Oxide Layer on Carbon Steel.

The best least-squares fitting resistance and capacitance values of the EIS results using the circuit, presented in Figure 11, show some general trends, Figure 12,13.

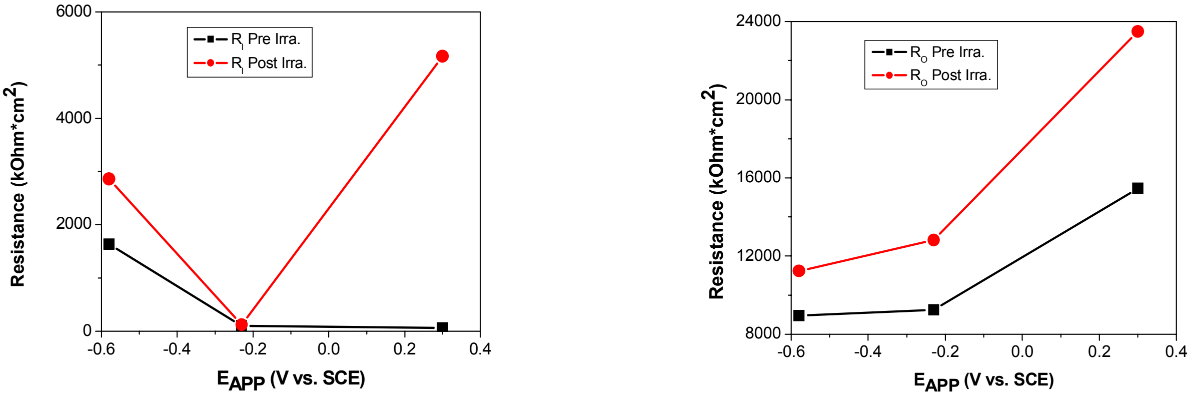

Figure 12: Changes in Film Resistances Due to 2 h Irradiation for Films Grown at Various Potentials, E_{APP}: (a) Resistance of the Inner $Fe^{II/III}$ Oxide Layer and (b) the Outer Fe^{III} Oxide Layer.

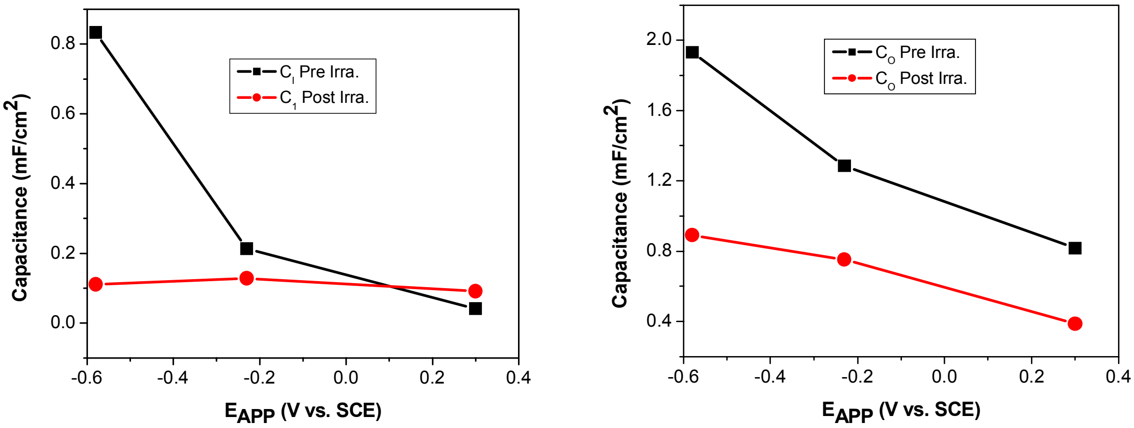

Figure 13: Changes in Film Capacitances Due to 2 h Irradiation for Films Grown at Various Potentials, E_{APP}: (a) Capacitace of the Inner $Fe^{II/III}$ Oxide Layer and (b) the Outer Fe^{III} Oxide Layer.

When both the Bode and Nyquist plots were fit to the equivalent circuit some general trends were seen. First, as expected, the outer layer had a much higher resistance in all cases since the outer layer is composed of Fe_2O_3 and FeOOH, which are more resistive than the Fe_3O_4 inner layer. Also, by performing EIS measurements before and after irradiation or the addition of hydrogen peroxide the effects of irradiation and hydrogen peroxide on carbon steel's oxides could be determined. It was seen that after a 2-h irradiation period the resistance of both layers increased and the capacitance of both layers decreased. The increase in the resistance (and corresponding decrease in capacitance) for both layers reflects a combination of film thickening and defect annealing (removing stresses). This matches with the increase in corrosion potential seen during irradiation, signifying iron was forming oxides of higher oxidation states, which are more resistive than the Fe_3O_4 layer. Also, a general trend of an increase in resistance for the outer layer as the film growth potential increased was seen, representing a thicker and more resistive Fe_2O_3 layer. Similar changes in magnitude were seen the cases of hydrogen peroxide addition.

4. CONCLUSION

The behaviour of E_{CORR} of carbon steel in water observed during exposure to γ-radiation was similar to that observed during the exposure to water with H_2O_2 added under non-irradiated conditions. This indicates the main influence of gamma radiation on carbon steel corrosion is via the radiolytic production of H_2O_2 in the aqueous phase. The effect of •OH, the other radiolytically produced oxidizing species on the carbon steel corrosion appears to be small.

It was also found that, for a given carbon steel surface, E_{CORR} is a function of $[H_2O_2]$ when $[H_2O_2]$ was less than 10^{-3} M. Once the response time of E_{CORR} of a given surface to a change in the H_2O_2 concentration is established, the change in E_{CORR} during the exposure to γ-radiation can be predicted if the radiolytic production of H_2O_2 is known.

The EIS analyses showed that the surface oxides on carbon steel comprise of a dual-layer structure with an inner magnetite and an outer hematite layer. The analyses before and after irradiation showed an increase in resistance and decrease in capacitance for both layers upon irradiation, consistent with the increase in E_{CORR} due to irradiation. These results indicate an increase in passivity of the carbon steel surface with irradiation.

5. FUTURE WORK

The study of the effects of radiation on the corrosion kinetics of carbon steel covered with preformed oxide films will continue, which will also include in-situ measurements of EIS. The effect of dissolved impurities, including Fe^{2+} and dissolved oxygen, on the radiolytic corrosion processes will be studied.

The final goal of the carbon steel corrosion study is to develop a kinetic model that can predict the corrosion potentials of carbon steel piping systems under radiation conditions. The corrosion potential on the carbon steel feeder pipes in a nuclear reactor is very difficult to monitor. A corrosion kinetics model, which can determine E_{CORR} as a function of the radiolytic redox species concentrations, either through the water radiolysis model or the analysis of the reactor water samples, will be of great value.

5. ACKNOWLEDGEMENT

This research was funded under the Natural Science and Engineering Council of Canada (NSERC) and Atomic Energy of Canada Limited (AECL) Industrial Research Chair Agreement. The electrochemical analysis equipment was purchased by a grant from the Canada Foundation for Innovation. Thanks are also due to Jiju Joseph and Xueyuan Zhang for their experimental support.

6. REFERENCES:

1. CANDU Reactors. 2007 March. Available from: http://www.aecl.ca/Reactors.htm

2. J.W.T. Spinks and R.J. Woods, Wiley-Interscience; 3 Sub edition, 243 (1990).

3. K. Ishigure, T. Nukii and S. Ono, Journal of Nuclear Materials , 350(1), 56 (2006).

4. C.C.Lin , Y.J. Kim , L.W. Niedrach, K.S. Ramp, CORROSION 52 (8), 618(1996)

5. J.C. Wren, J.M. Ball, Radiation Physics and Chemistry 60, 577–596 (2001).

6. R.M. Cornell and U. Schwertmann, The Iron Oxides, 2nd ed, Wiley-Vch Gmbh, 210 (2000).

7. D.J. Jobe, R. J. Lemire and P. Taylor, Iron oxide redox chemistry and nuclear fuel disposal, AECL-11667, COG-96-487-1 (1997).

8. D.J. Jobe, The calculated solubilities of hematite, magnetite and lepidocrocite in steam generator feedtrains, AECL-11683 (1997).

9. Radioactive material data sheet. 2007 March. [cited March 12, 2007]. Available from: http://www.stuarthunt.com/Downloads/RMSDS/Co60.pdf

10. A.J. Bard and L.R. Faulkner, Electrochemical methods: Fundamentals and applications, 2nd edition, John Wiley & Sons, 2001.

11. M. Buchler, P. Schmuki and H. Bohni, J. Electrochem. Soc. 145, 609 (1998).

12. M. Buchler, P. Schmuki and H. Bohni, J. Electrochem. Soc. 144, 2307 (1997).

13. A. Hugot-LeGoff, J. Flis, N Boucherit, S. Joriet and J. Wilimski , J. Electrochem. Soc. 137, 2684 (1990).

14. X. Zhang, W. Xu, D.W. Shoesmith and J.C. Wren, Kinetics of H_2O_2 reaction with oxide films, Corrosion Science, Submitted.

15. R.S.S. Gusman, J.R. Vilche and A.J. Arvia, Electrochim. Acta, 24, 395 (1979).

16. D.C. Silverman, Corrosion, 38(8), 453 (1982).

17. R07 Table showing several standard reduction potentials. 2007 March. Available from: http://www.iupac.org/didac/Didac%20Eng/Didac03/Content/R07.htm

18. E. Barsoukov and J.R. Macdonald, Impedance Spectroscopy, 2nd edition, John Wiley & Sons, 2005.